Wavenumber broadening of the quasi 2 day planetary wave in the ionosphere

Jia Yue,[1] Wenbin Wang,[2] Arthur D. Richmond,[2] Han-Li Liu,[2] and Loren C. Chang[3]

Received 15 November 2012; revised 2 April 2013; accepted 29 April 2013; published 3 June 2013.

[1] Using the Thermosphere Ionosphere Mesosphere Electrodynamics General Circulation Model, we investigate the observed zonal wavenumber broadening phenomena in the ionospheric quasi 2 day oscillation (QTDO) that is associated with westward zonal wavenumber 3 (W3) quasi 2 day wave (QTDW) perturbations in the mesosphere and lower thermosphere (MLT). We aim to explain why the observed longitudinal structures of the QTDOs in the ionosphere are different from those of the QTDWs in the MLT. We find that large QTDOs in the ionosphere with zonal wavenumbers other than W3 occur in the model run with the true magnetic field, but not in the model run with an aligned dipole field. These numerical experiments suggest that the occurrence of the additional zonal wavenumbers in ionospheric QTDOs is related to the longitudinal variations of the Earth's magnetic field configuration, strength, and dip angle, which have distinct stationary zonal wavenumbers. We also find that when the specified W3 QTDW winds drive ionospheric plasma motion in the magnetic field, the resultant QTDOs in ionospheric parameters, such as the dynamo electric field, ion vertical drifts, plasma densities, and total electron content, have more complicated longitudinal variations than simply W3, corresponding to a zonal wavenumber broadening effect. Additionally, we find that the wavenumber broadening effect in the ionosphere can be fed back onto the neutrals through ion drag, to produce small QTDW winds with new wavenumbers in the thermosphere.

Citation: Yue, J., W. Wang, A. D. Richmond, H.-L. Liu, and L. C. Chang (2013), Wavenumber broadening of the quasi 2 day planetary wave in the ionosphere, *J. Geophys. Res. Space Physics*, *118*, 3515–3526, doi:10.1002/jgra.50307.

1. Introduction

[2] Coordinated ground-based and space-borne observations have shown that quasi 2 day variability in the geomagnetic field, the equatorial electrojet, and ionospheric *F*-region electron densities is correlated with the quasi 2 day wave (QTDW) in the neutral wind and temperature fields in the mesosphere and lower thermosphere (MLT) region during geomagnetically quiet times [e.g., *Pancheva et al*., 1994, 2006; *Gurubaran et al*., 2001; *Takahashi et al*., 2005; *Lastovicka*, 2006; *Chang et al*., 2011a]. For instance, *Pancheva et al*. [1994, 2006] observed that quasi 2 day oscillations (QTDOs) were present in both the MLT and the ionosphere. They showed that during the time when quasi 2 day fluctuations were prominent in the MLT, similar variations were observed in the ionosphere. *Chang et al*. [2011a] also reported concurrent westward wavenumber 2 (W2) and westward wavenumber 3 (W3) QTDWs in the MLT temperature and quasi 2 day fluctuations with similar longitudinal features in the ionospheric total electron content (TEC).

[3] Recently, *Yue et al*. [2012b] simulated the modulation of the ionosphere by the QTDW, using the three-dimensional first-principles Thermosphere Ionosphere Mesosphere Electrodynamics General Circulation Model (TIME-GCM). The QTDW in the MLT was realistically reproduced in the TIME-GCM, when compared to satellite observations [e.g., *Wu et al*., 1993]. As shown by *Yue et al*. [2012b], the QTDW modulates the *E*-region neutral wind dynamo at southern middle latitudes. The resultant QTDO of electric fields is mapped to the Northern Hemisphere, producing QTDOs of vertical ion drift at both low and middle latitudes and QTDOs of the equatorial fountain effect in the ionosphere. Therefore, ionospheric plasma density and TEC at the dip equator and near the Equatorial Ionization Anomaly (EIA) crests are modulated at a quasi 2 day period. The modeled QTDO structures of TEC are consistent with ionospheric observations [*Forbes and Zhang*, 1997; *Chen*, 1992; *Chang et al*., 2011a].

[4] The numerical study by *Yue et al*. [2012b], along with the work by *Ito et al*. [1986] and *Chen* [1992], gives a plausible mechanism by which the QTDW modulates the ionospheric *E*-region dynamo, the equatorial fountain effect, middle and low latitude ion drifts, EIA ionospheric plasma densities, and TEC. There are, however, many important aspects of the coupling between QTDWs and the ionosphere that have not been fully understood. The current paper aims

[1]Atmospheric and Planetary Science, Hampton University, Hampton, Virginia, USA.
[2]High Altitude Observatory, National Center for Atmospheric Research, Boulder, Colorado, USA.
[3]Institute of Space Science, National Central University, Jhongli, Taiwan.

Corresponding author: J. Yue, Atmospheric and Planetary Science, Hampton University, Hampton, VA 23668, USA. (jia.yue@hamptonu.edu)

2169-9380/13/10.1002/jgra.50307

Table 1. List of Four TIME-GCM Runs Performed in This Paper

Runs	Run Name	QTDW Forced at Model Lower Boundary	Dynamo	Magnetic Field
1	Standard	Yes	Yes	IGRF
2	Control run 1: no dynamo	Yes	No	IGRF
3	Control run 2: aligned magnetic dipole	Yes	Yes	Aligned pure dipole
4	Base	No	Yes	IGRF

to address one of the open questions concerning this coupling: the obvious differences between the longitudinal structures of the QTDOs in the ionosphere and those of the QTDWs in the MLT region. Although the quasi 2 day oscillation period is the same in the MLT and ionosphere, the zonal wavenumbers of this oscillation have been observed to be very different in these two regions [*Apostolov et al*., 1995; *Forbes and Zhang*, 1997]. A prominent component of the QTDW in both austral and boreal summers in the MLT has zonal W3 [*Salby*, 1981]. W2 and W4 components are also evident but have smaller amplitudes [*Tunbridge et al*., 2011]. In general, the QTDW in the MLT has typical longitudinal wavenumbers ranging from W2 to W4. On the other hand, based on their analysis from multiyear ionosonde observations, *Apostolov et al*. [1995] and *Forbes and Zhang* [1997] observed strong W1 and stationary (S0) QTDOs of the ionospheric *F*-region peak plasma density (NmF2) at midlatitudes. At low latitudes, a broader spectrum of wavenumbers (E2 to W4) was found in NmF2 [*Forbes and Zhang*, 1997]. The occurrence of E2, E1, S0, and W1 components in the ionospheric QTDOs cannot be simply attributed to the W2–W4 QTDW wind perturbations in the MLT region.

[5] In this paper, we examine the effect of the displacement between geographic poles and magnetic poles on the zonal wavenumber response of the ionospheric QTDOs to the QTDW perturbations in the MLT, using TIME-GCM simulations. We perform numerical experiments to elucidate the mechanisms responsible for the differences between the zonal wavenumbers of the QTDW in the MLT and those of the QTDO in the *E* and *F*-region ionosphere, as observed by *Apostolov et al*. [1995] and *Forbes and Zhang* [1997].

2. TIME-GCM and Numerical Experiments

[6] Following *Palo et al*. [1998], *Liu et al*. [2004], *Chang et al*. [2011b], and *Yue et al*. [2012a, 2012b], the TIME-GCM is employed here to conduct numerical experiments related to the QTDW. The TIME-GCM is a self-consistent, time-dependent, three-dimensional model [*Roble et al*., 1988; *Richmond et al*., 1992; *Roble and Ridley*, 1994]. The TIME-GCM calculates global neutral winds, temperature, constituents, electron and ion densities, temperatures and drifts, and the dynamo electric field from the upper stratosphere (~30 km) to the thermosphere (~500 km). The grid size is $5^\circ \times 5^\circ$ in latitude and longitude and one-half scale height in the vertical, with a time step of 2 min. For this study, the background field is set to a perpetual 15 January state, when the QTDW reaches its maximum amplitude in the midlatitude summer mesosphere [e.g., *Wu et al*., 1993]. The amplitudes and phases of the migrating diurnal and semidiurnal tides at the model lower boundary are input from the Global Scale Wave Model (GSWM) [*Hagan et al*., 1999]. Since the TIME-GCM cannot generate QTDWs internally, a constant W3 QTDW forcing with a 48 h period in geopotential is also specified at the model lower boundary from the beginning of the model simulations, with no other wavenumbers being imposed. Furthermore, no nonmigrating tides or other planetary waves are forced. The neutral wind dynamo electric field is solved using self-consistently calculated neutral winds and ionospheric conductivities [*Richmond et al*., 1992]. The model is under solar minimum (F10.7 = 75 solar flux unit (sfu)) and quiet geomagnetic activity conditions ($Kp = 0$). The model runs over 30 days for each case as described below.

[7] Four TIME-GCM runs are conducted in this study (cf. Table 1). The first is the standard run with the GSWM tides and W3 QTDW forced at the model lower boundary and the *E*-region dynamo effect enabled. Two control runs are conducted with altered TIME-GCM settings. For the first control run, the dynamo electric fields are disabled, while the QTDW is still forced at the model lower boundary. This run is to demonstrate the key role played by the *E*-region dynamo in the coupling between the QTDW and the ionosphere. Both the standard run and the first control run implement actual geomagnetic field (i.e., the International Geomagnetic Reference Field (IGRF) [*International Association of Geomagnetism and Aeronomy*, 2010]). In the second control run, we change the Earth's magnetic field from the IGRF to a pure magnetic dipole field aligned with the Earth's geographic axis. In the aligned magnetic dipole case, all the magnetic anomalies, such as the South Atlantic Anomaly [*Gledhill*, 1976], are absent and the magnetic and geographic coordinates completely coincide. Thus, the magnetic field strength and dip angle do not change with longitude at the same geographic latitude. This second control run is to illustrate the importance of the configuration of the magnetic field in the response of the ionosphere to QTDWs. Additionally, a base run is conducted, which is identical to the standard run except that no QTDWs are imposed at the model lower boundary.

3. Simulation Results

[8] In this work, TIME-GCM outputs of temperature, wind, electric fields, vertical ion drift, and TEC at all geographic (or magnetic) longitudes and universal times are analyzed. The magnitudes and phases of the QTDW of these parameters in the MLT and their QTDO in the ionosphere are retrieved with a 2 day sliding window. Using the least squares fitting algorithm of *Wu et al*. [1993], the TIME-GCM outputs are fitted to a function of the form:

$$F(\lambda,t) = \overline{F} + \sum_{n=1}^{2}\sum_{s=-4}^{4} \widehat{F}_{n,s}\, cos\left(n\Omega t - s\lambda - \widehat{\psi}_{n,s}\right) + \sum_{s=-5}^{2} \widehat{F}_{\mathrm{QTDW}}\, cos\left(\Omega t/2 - s\lambda - \widehat{\psi}_{\mathrm{QTDW}}\right) \quad (1)$$

where λ is longitude, t is universal time, $\Omega = \frac{2\pi}{24}\,\mathrm{h}^{-1}$, and s is the zonal wavenumber. $\overline{F}$ is the zonal mean value. The

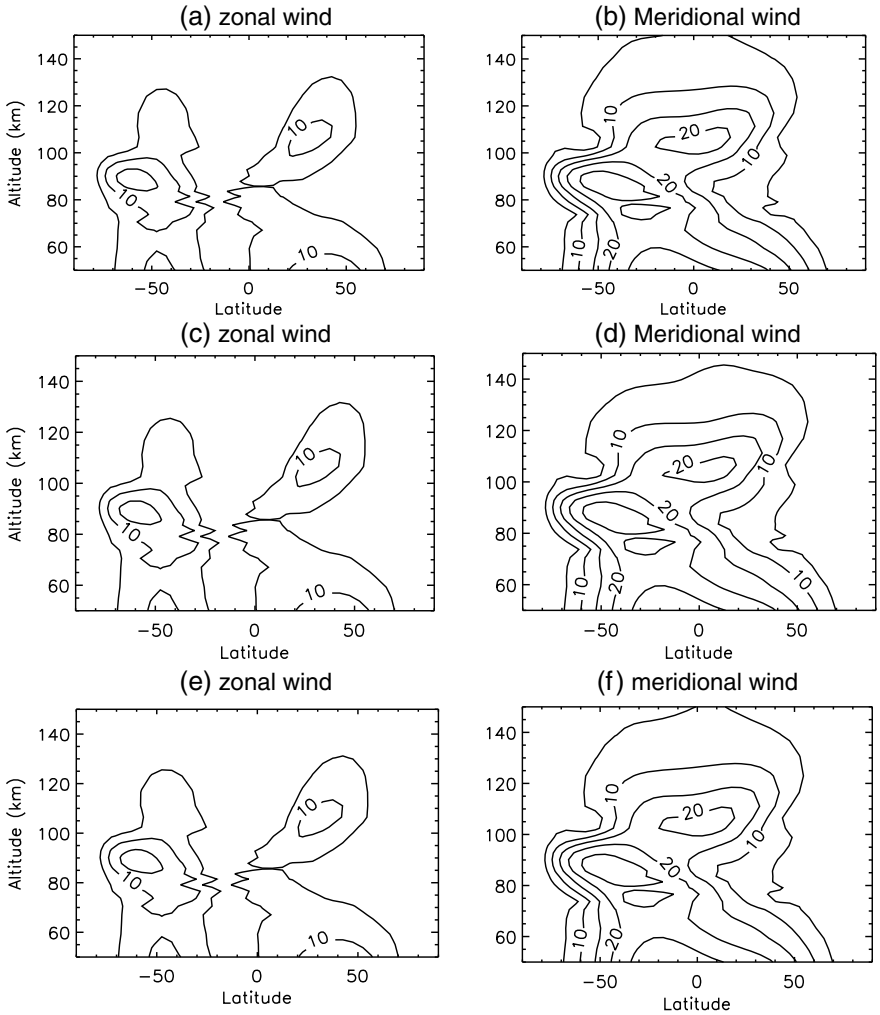

Figure 1. The amplitudes of the W3 QTDW in (left) zonal and (right) meridional winds as a function of geographic latitude and altitude on model days 27–28, obtained using least squares fitting of the TIME-GCM output, as described in the text. The QTDW components in the standard run, the control run with dynamo turned off, and the run with aligned magnetic dipole are shown in the top, middle, and bottom rows, respectively. The contour interval is 5 m s^{-1}.

second term accounts for diurnal and semidiurnal tides with zonal wavenumbers from W4 ($s = -4$) to E4 ($s = 4$). n = 1, and 2 denotes the diurnal and semidiurnal tide, respectively. The third term represents the QTDW with zonal wavenumbers of W5 ($s = -5$) to E2 ($s = 2$). $\widehat{F}$ and $\widehat{\psi}$ are the fitted amplitude and phase for each component. Since there are no other planetary waves that are either forced at the model lower boundary or generated within the TIME-GCM, they are not included in equation (1).

[9] The TIME-GCM runs take about 15 days to become completely stable. After 15 days, the simulated QTDW response is relatively invariant from day to day and repeatable till the end of the model runs (day 30). Figure 1 displays the amplitudes of the W3 QTDW in zonal and meridional winds on model days 27–28 for the standard run (top row), the first control run with dynamo disabled (middle row), and the second control run with aligned dipole (bottom row). (There is no noticeable QTDW in the base run (not shown in Figure 1) because the QTDW is not forced at the model lower boundary in this case.) As shown in Figure 1, the QTDW perturbations in the neutral winds are essentially identical below about 120 km in all three runs. The zonal wind perturbation of the QTDW exhibits two peaks of 10–15 m s^{-1} at middle latitudes in both hemispheres. The meridional wind of the QTDW shows one peak of 30 m s^{-1} near 90 km at southern middle latitudes and another peak of 20 m s^{-1} in the equatorial lower thermosphere. These features of the simulated QTDW are in agreement with satellite observations [e.g., *Wu et al*., 1993; *Limpasuvan et al*., 2005] and prior TIME-GCM simulations [e.g., *Liu et al*., 2004; *Chang et al*., 2011b; *Yue et al*., 2012a, 2012b]. The QTDW in meridional wind above 140 km in the run with dynamo off (Figure 1d) is slightly weaker than those in the other two runs (Figures 1b and 1f). Figure 1 also shows that the QTDW perturbations of neutral winds are almost identical in the standard run (top row) and the control run with aligned dipole (bottom row). Therefore, the geometry of the magnetic field has almost no influence on the W3 QTDW in the MLT region.

[10] Figure 2 displays the QTDW meridional wind components with wavenumbers other than W3 in geographic

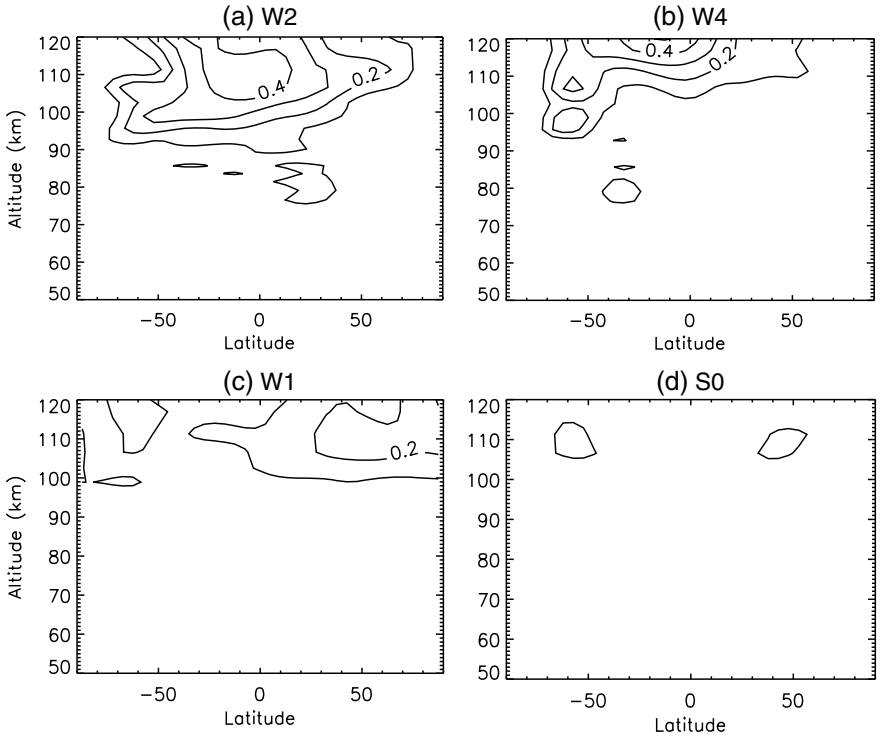

Figure 2. Amplitudes of the QTDW meridional components with wavenumbers other than W3 in the standard run, as a function of geographic latitude and altitude, on days 27–28, (a) for westward propagating wavenumber 2, (b) for westward propagating wavenumber 4, (c) for westward propagating wavenumber 1, and (d) for stationary wavenumber 0. The contour interval is 0.1 m s^{-1}.

coordinates in the standard run. (Note that all of the QTDW and QTDO in this paper are plotted in geographic coordinates, except Figure 4.) The zonal wind components are much smaller and are not shown here. The W2 and W4 QTDWs have slightly larger amplitudes (~0.4 m s^{-1}) in the lower thermosphere than the W1 and S0 ones. Nevertheless, all of the QTDWs with wavenumbers other than W3 are negligible (less than 0.4 m s^{-1}) below 100 km, compared to the W3 QTDW (~20 m s^{-1}) shown in Figure 1. This is expected because QTDWs with wave numbers other than W3 are neither forced at the lower boundary of the TIME-GCM nor generated internally. Above ~100 km, the QTDWs with other wavenumbers become noticeable due to the ion-drag effect from the ionosphere, which will be discussed later.

[11] As described by *Ito et al*. [1986], *Chen* [1992], and *Yue et al*. [2012b], the QTDW modulates the mean wind in the *E*-region and pushes plasma to move perpendicular to the magnetic field in a period of 2 days and produces a 2 day perturbation in the dynamo electric fields. The QTDW-perturbed dynamo electric fields are largely controlled by the Earth's magnetic field and follow geomagnetic coordinates [*Richmond*, 1995; *Heelis*, 2004]. Therefore, the QTDW-induced oscillations in electric fields and vertical

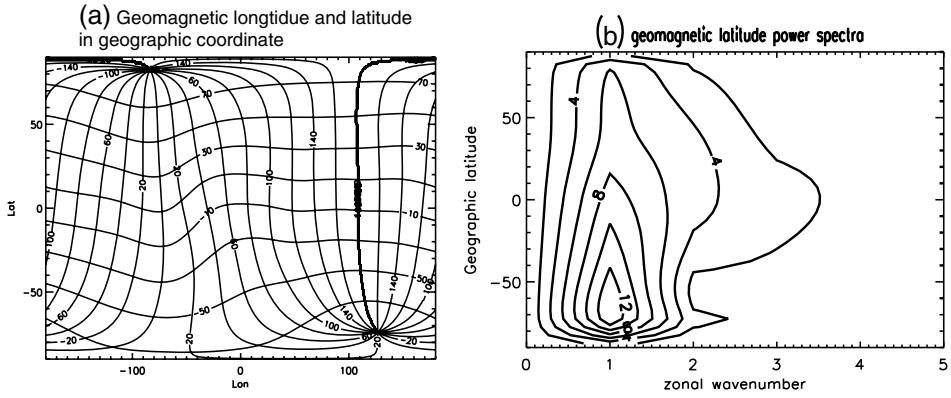

Figure 3. (a) Earth's magnetic longitude and latitude (in degrees) in geographic coordinates, (b) Fourier spectrum of the magnetic latitude (in degrees) with respect to geographic longitude as a function of geographic latitude. Zonal mean values are removed in Figure 3b.

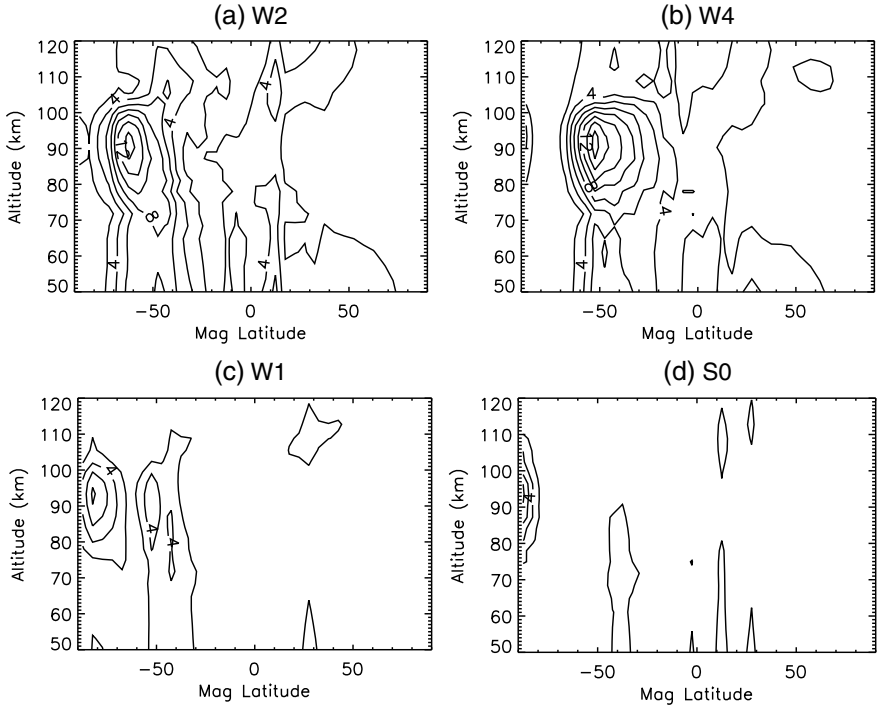

Figure 4. Amplitudes of QTDW meridional wind components with wavenumbers other than W3 in the standard run, as a function of geomagnetic latitude and altitude on days 27–28: (a) for W2, (b) for W4, (c) for W1, and (d) for S0. The contour interval is 2 m s^{-1}.

ion drift are often calculated in geomagnetic coordinates [e.g., *Chang et al*., 2011a], while the QTDW in winds is better described in geographic coordinates [e.g., *Wu et al*., 1993]. When the QTDW winds are mapped from geographic to magnetic coordinates, QTDWs of wavenumbers other than W3 can show up [*Chang et al*., 2011a], even though there is no actual change in the QTDW winds.

[12] Figure 3a displays geomagnetic longitude and latitude in geographic coordinates. There is a distinct wavenumber 1 variation in magnetic latitude, which is more pronounced in the Southern Hemisphere. Figure 3b shows the Fourier spectrum of the magnetic latitude at geographic latitude with the zonal mean values being removed. The power spectrum has a strong wavenumber 1 component near 50°S –70°S and higher wavenumbers (2 and 3) at the tropics, corresponding to the differences between the two coordinate systems shown in Figure 3a. As a result, a field with no longitudinal variations in geographic coordinates will show zonal structures in geomagnetic coordinates and vice versa. Thus, when the W3 QTDW is "projected" from geographic coordinates to geomagnetic coordinates, this coordinate transformation mimics an "interaction" between the original W3 structure of the QTDW and a stationary wave 1 (S1) feature in geomagnetic coordinates (Figure 3b). The "new" QTDW components in geomagnetic coordinates have wavenumbers that are sums and differences between the original wave number of the QTDW and the zonal wavenumbers in the magnetic field, which is similar to the mathematical treatment in *Teitelbaum and Vial* [1991]. Because the magnetic field is stationary, the periods of the "new" waves remain quasi 2 day. QTDW components of wind perturbations with additional wavenumbers, such as W3 ± S1 = W2 and W4, etc., are "created" in magnetic coordinates. Figure 4 illustrates this effect by plotting the QTDW meridional wind components with W2, W4, W1, and S0 in magnetic coordinates. In Figures 4a and 4b, the "new" W2 and W4 QTDWs have peaks of 14 m s^{-1} at 90 km and at 50°S–60°S, corresponding to the strong S1 feature of the magnetic field around 50°S–70°S (see Figure 3b). The "new" W1 component is ~4 m s^{-1} at 90 km around 50°S (Figure 4c), and the "new" S0 component is smaller (Figure 4d). Compared to the QTDWs in geographic coordinates from Figure 2, the QTDWs with wavenumbers other than W3 in geomagnetic coordinates are much more pronounced and occur mostly below 100 km. (Note that the transformation between geographic and magnetic coordinates is totally reversible for the QTDW wind. When all wavenumber components of the QTDW in magnetic coordinates are combined in geographic coordinates, only the W3 QTDW is seen.)

[13] The geomagnetic field strength **B** also displays longitudinal structures in both geographic and geomagnetic coordinates. Figure 5a exhibits the magnetic field strength in geographic coordinates. The **B** field shows a strong wave number 1 feature that peaks around 50°S because of the South Atlantic Anomaly, where the Earth's magnetic field strength is the weakest [*Gledhill*, 1976]. In the Southern Hemisphere, the maximum of the **B** field occurs near the coast of Antarctica and south of Australia, as shown in Figure 5a. On the other hand, the **B** field strength has a distinct zonal wavenumber 2 feature at northern midlatitudes, because of the two maxima over northern Canada and Siberia. Similar to Figure 3b, we calculate the Fourier spectrum of the field strength in geographic coordinates in Figure 5b, with the zonal mean values being removed. Figure 5b shows that the **B** field can be decomposed into different wavenumber components, with a strong wave

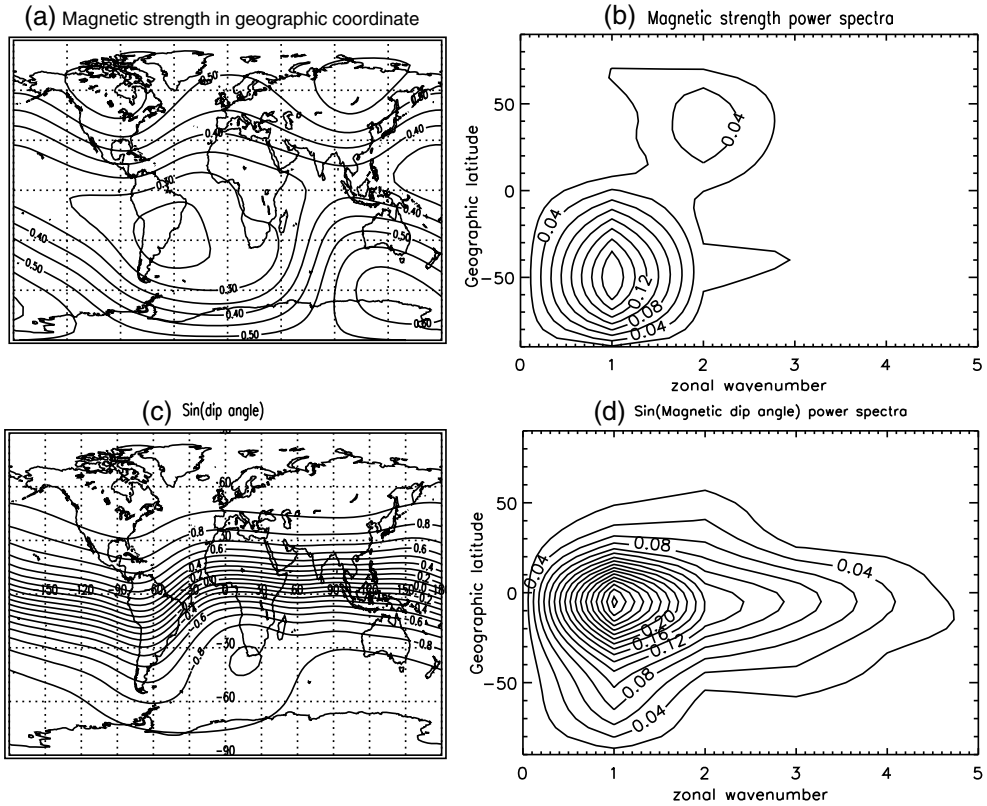

Figure 5. (a) Earth's magnetic field strength (in Gauss) in geographic coordinates, (b) Fourier spectrum of the magnetic field (in Gauss) as a function of geographic latitude. (c) Sine function of the magnetic dip angle in geographic coordinates. (d) Fourier spectrum of the sine function of the magnetic field dip angle. Zonal mean values are removed in Figures 5b and 5d.

number 1 feature in the Southern Hemisphere corresponding to the South Atlantic Anomaly and a wavenumber 2 feature in the Northern Hemisphere. These wavenumbers of the magnetic field strength also exist in magnetic coordinates, although with different amplitudes. Similarly, Figure 5c exhibits the sine of the magnetic dip angle I, sin(I), in geographic coordinates. A wavenumber 1 feature is evident at low and mid latitudes. The power spectrum of sin(I) is shown in Figure 5d with the zonal mean value removed. The zonal wavenumber 1 feature is distinct along with higher wavenumbers at low latitudes through southern midlatitudes. These longitudinal structures of sin (I) also exist in magnetic coordinates, although with smaller amplitudes.

[14] The QTDW can produce relative motions between the ions and electrons in the E-region, which modulates dynamo currents and electric fields [*Ito et al*., 1986]. The QTDOs of the wind-driven Hall and Pedersen currents in the magnetic eastward direction, J_x, are [*Liu et al*., 2010]

$$J^{W,H}_{x,\mathrm{QTD}} = \sigma_H u_{\mathrm{QTDW}} B \tag{2}$$

$$J^{W,P}_{x,\mathrm{QTD}} = \sigma_P v_{\mathrm{QTDW}} B \sin(I) \tag{3}$$

where σ_H and σ_P are the Hall and Pedersen conductivities and u_{QTDW} and v_{QTDW} are the magnetic eastward and northward components of the QTDW wind. Note that the QTDW has multiple wavenumbers (W2, W3, W4, etc.) in magnetic coordinates, due to the transformation from geographic to geomagnetic coordinates, as shown in Figure 4. Both the magnetic field strength **B** and the magnetic dip angle I have multiple zonal wavenumbers in both geographic and magnetic coordinates. In particular, the stationary wavenumber 1 (S1) zonal structure is substantial at low and middle latitudes in the Southern Hemisphere. From equations (2) and (3), we can see that zonal wavenumber summations and subtractions take place between the QTDW winds (u_{QTDW}, v_{QTDW}), **B**, and sin(I), leading to multiple zonal wavenumbers in the currents J_x:

$$\begin{aligned} &\mathrm{W3} \pm \mathrm{S1} = \mathrm{W2}, \mathrm{W4} \\ &\mathrm{W2} \pm \mathrm{S1} = \mathrm{W1}, \mathrm{W3} \\ &\mathrm{W3} \pm \mathrm{S2} = \mathrm{W1}, \mathrm{W5} \\ &\text{etc.} \end{aligned} \tag{4}$$

[15] The accumulation of polarization charges in the E-region is modulated as the QTDW wind pushes the plasma back and forth perpendicular to magnetic field lines, which can be written as the zonal convergence of the Hall and Pedersen currents, $-\partial\left(J^{W,H}_x + J^{W,P}_x\right)/\partial x$ [*Heelis*, 2004]. Since the currents J_x have new zonal wavenumbers, as shown in equation (4), the polarization charges and the resultant electric potential Φ of the polarization electric fields also have new zonal wavenumbers.

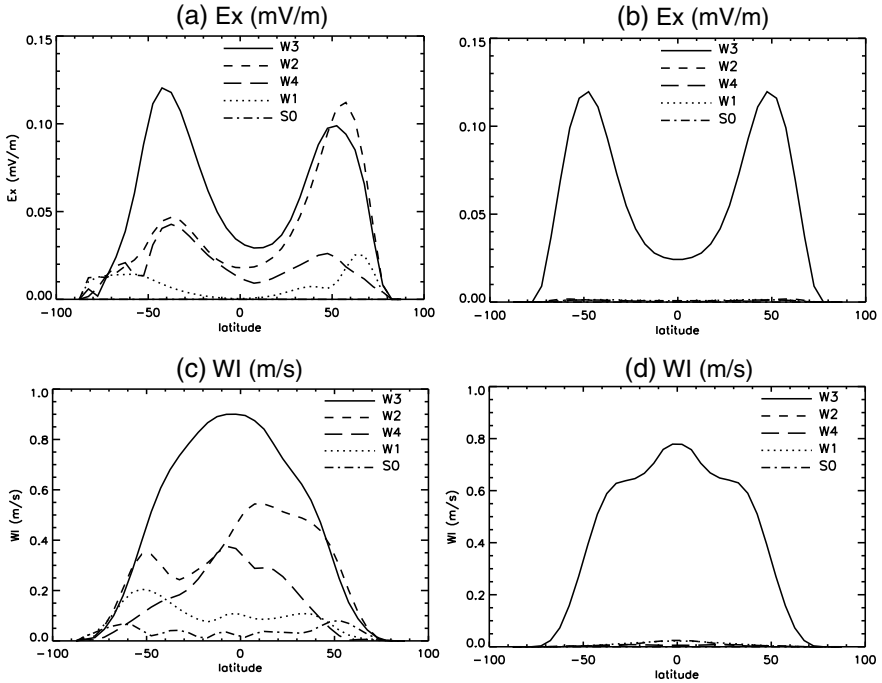

Figure 6. Different wavenumber components of QTDOs of electric fields (in mV/m) at 120 km in the geographic zonal direction on days 27–28 as a function of geographic latitude (a) in the standard run using the IGRF magnetic field and (b) in the control run using an aligned dipole magnetic field. Different wave number components of QTDOs of the vertical ion drift (in m/s) with respect to the field line at 300 km as a function of geographic latitudes (c) for the standard run using the IGRF magnetic field and (d) for the test run using the aligned dipole magnetic field. The solid lines, short dashed lines, long dashed lines, dotted lines, and dash-dotted lines denote the W3, W2, W4, W1, and S0 components, respectively.

[16] The electric polarization fields are calculated from the gradient of the electric potential [e.g., *Heelis*, 2004; *Yue et al*., 2012b]:

$$\overrightarrow{E}(s) = -\nabla\Phi \tag{5}$$

[17] Because Φ has multiple zonal wavenumbers in both geographic and magnetic coordinates, the electric fields also possess wavenumbers other than W3. Figures 6a and 6b show the QTDO of electric field in the geographic zonal direction, E_x, at 120 km on days 27–28, in the standard TIME-GCM run with the IGRF magnetic field configuration (Figure 6a) and in the control run with the aligned dipole (Figure 6b). Figure 6a shows that along with the W3 QTDO (solid line) of E_x, the W2, W4, and W1 components are all non-negligible. On the other hand, in the control run with an aligned magnetic dipole field, only the W3 QTDO of E_x is significant and QTDOs with other zonal wavenumbers are not noticeable, as shown Figure 6b. This demonstrates clearly that the creation of new zonal wavenumber components in QTDO electric fields can be fully accounted for by the configuration of the magnetic field that results from the displacement between magnetic poles and geographic poles and the strong non-dipolar component of the Earth's magnetic field, such as the South Atlantic Anomaly. (Note that in the first control run with the dynamo disabled, the electric field is zero for all wavenumbers.) The creation of new zonal wavenumbers in the QTDO, such as W2, W1, W4, and S0, is physical and more complex than just a transformation between geographic and magnetic coordinates. It involves the dynamic coupling between neutral winds, ionospheric plasma motion, Earth's magnetic field and ionospheric currents and electric fields, as shown by equations (1)–(4). The new zonal wavenumber components of the QTDO of electric fields are substantial in both geographic coordinates (Figure 6a) and magnetic coordinates (not shown). This is different from the QTDW neutral winds in the MLT, which have large components with zonal wave numbers other than the specified W3 occurring only in magnetic coordinates but not in geographic coordinates.

[18] The QTDO of the dynamo electric field with multiple wavenumbers in the *E*-region can be transmitted to the *F*-region along the magnetic field lines [e.g., *Chen*, 1992; *Yue et al*., 2012b, and references therein]. It is the $\mathrm{E} \times \mathrm{B}$ ion drift, rather than the electric field itself, that has a direct influence on the ionosphere. Therefore, along with the wavenumber broadening of the electric fields, the vertical component of the resultant $\mathrm{E} \times \mathrm{B}$ ion drift includes further effects of wave number "interactions" between the QTDO of electric fields and the **B** field. Figures 6c and 6d show the QTDO of the vertical ion drift with different wavenumbers in geographic coordinates, in the standard run with the IGRF magnetic field configuration (Figure 6c) and the control run with the aligned magnetic dipole field (Figure 6d). Figure 6c illustrates that along with the W3 QTDO of 0.9 m s^{-1} in the vertical $\mathrm{E} \times \mathrm{B}$ drift at low latitudes, W2 (short dashed line, 0.5 m s^{-1}), W4 (long dashed line, 0.4 m s^{-1}), W1 (dotted line, 0.2 m s^{-1}), and S0 (dash-dotted line, 0.1 m s^{-1}) components are all significant at different latitudes. The W2 and W4 QTDOs of the

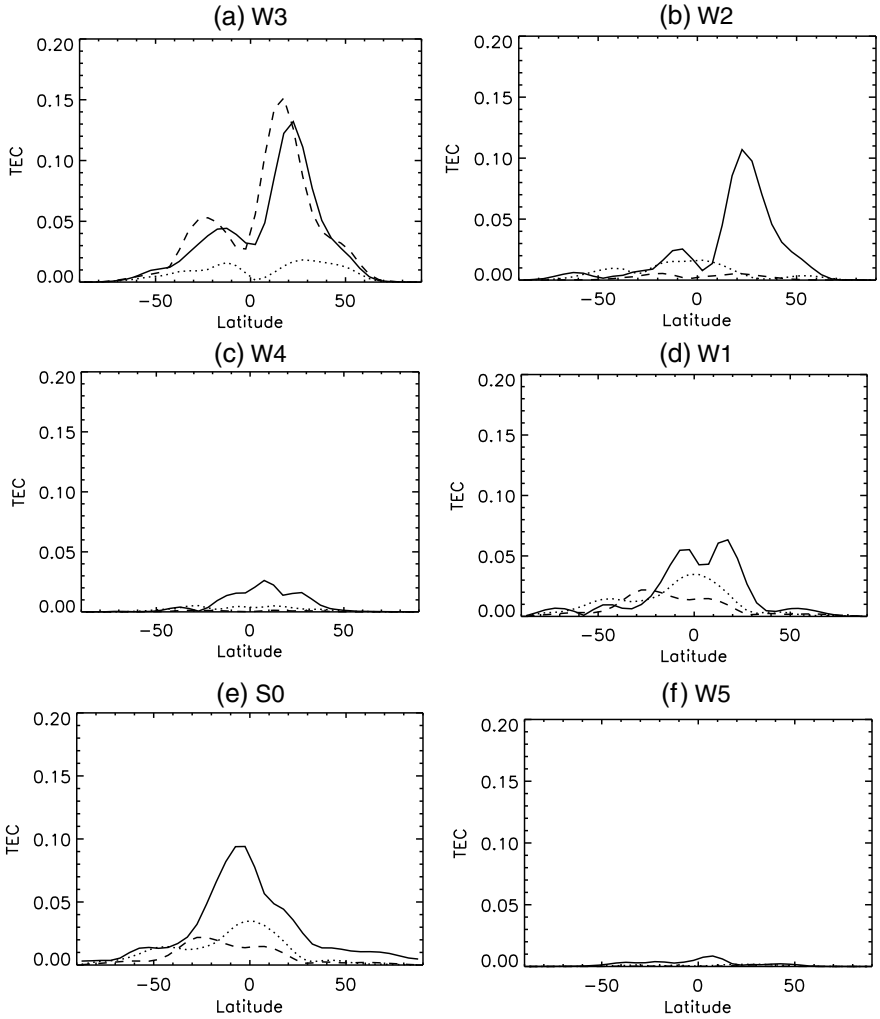

Figure 7. QTDW response in TEC (unit: TECU) as a function of geographic latitude with zonal wave number (a) W3, (b) W2, (c) W4, (d) W1, (e) S0, and (f) W5 on days 27–28. The solid lines are from the standard run results using the IGRF magnetic field. The dashed lines are results from the run using an aligned dipole magnetic field. The dotted lines denote the TECs for the test run with the dynamo off and in the IGRF magnetic field.

E × B drift are greater than the W1 and S0 components. This is probably related to the strong wavenumber 1 component in the magnetic field orientation and strength (see Figure 5), as shown by equation (4). On the other hand, in the control run with the aligned magnetic dipole field, only the W3 QTDO of the vertical ion drift is seen and other QTDO components are negligible (Figure 6d). In the control run with dynamo disabled and the base run without W3 QTDW forcing at the TIME-GCM lower boundary, there are no QTDOs in ionospheric electric field *E*. Therefore in these cases, there are no W3 and other wavenumber QTDOs of vertical E × B drift.

[19] A longitudinal modulation of the vertical plasma drift results in longitudinal structures of the plasma density and TEC in the *F*-region [e.g., *Chen*, 1992; *Immel et al*., 2006; *England et al*., 2006; *Hagan et al*., 2007]. Consequently, new zonal wavenumber components in the vertical ion drift lead to QTDOs of *F*-region plasma density and TEC with these wavenumbers. Figure 7 shows the QTDO of TEC with multiple zonal wavenumbers in the standard run and two control runs in geographic coordinates on days 27–28. (There is no QTDO of TEC in the base run.) In Figures 7a and 7b, the TEC response of W3 and W2 in the standard run has two peaks near the EIA crests (25°N and 15°S), which is in agreement with *Chen* [1992] and *Yue et al*. [2012b]. Comparing the results between the cases in the standard run (solid lines) and the aligned magnetic dipole field (dashed lines), we can see that QTDOs with new zonal wave numbers, especially W2 and W4 in Figures 7b and 7c, are much larger in the standard run than those with the aligned magnetic dipole. As shown in Figure 7b, the W2 QTDO of TEC reaches 0.1 TECU at northern midlatitudes in the standard run (solid line), whereas it is less than 0.01 TECU in the run with the aligned dipole field (dashed line). The W2 QTDO of TEC at southern latitudes is smaller because the W3 QTDO of TEC is weaker at southern latitudes [*Yue et al*., 2012b]. Similarly in Figure 7c, the W4 QTDO has a maximum of 0.03 TECU in the standard run (solid line), but its counterpart in the aligned dipole field (dashed line) is nearly zero. In Figures 7d–7f, the W1, S0, and W5

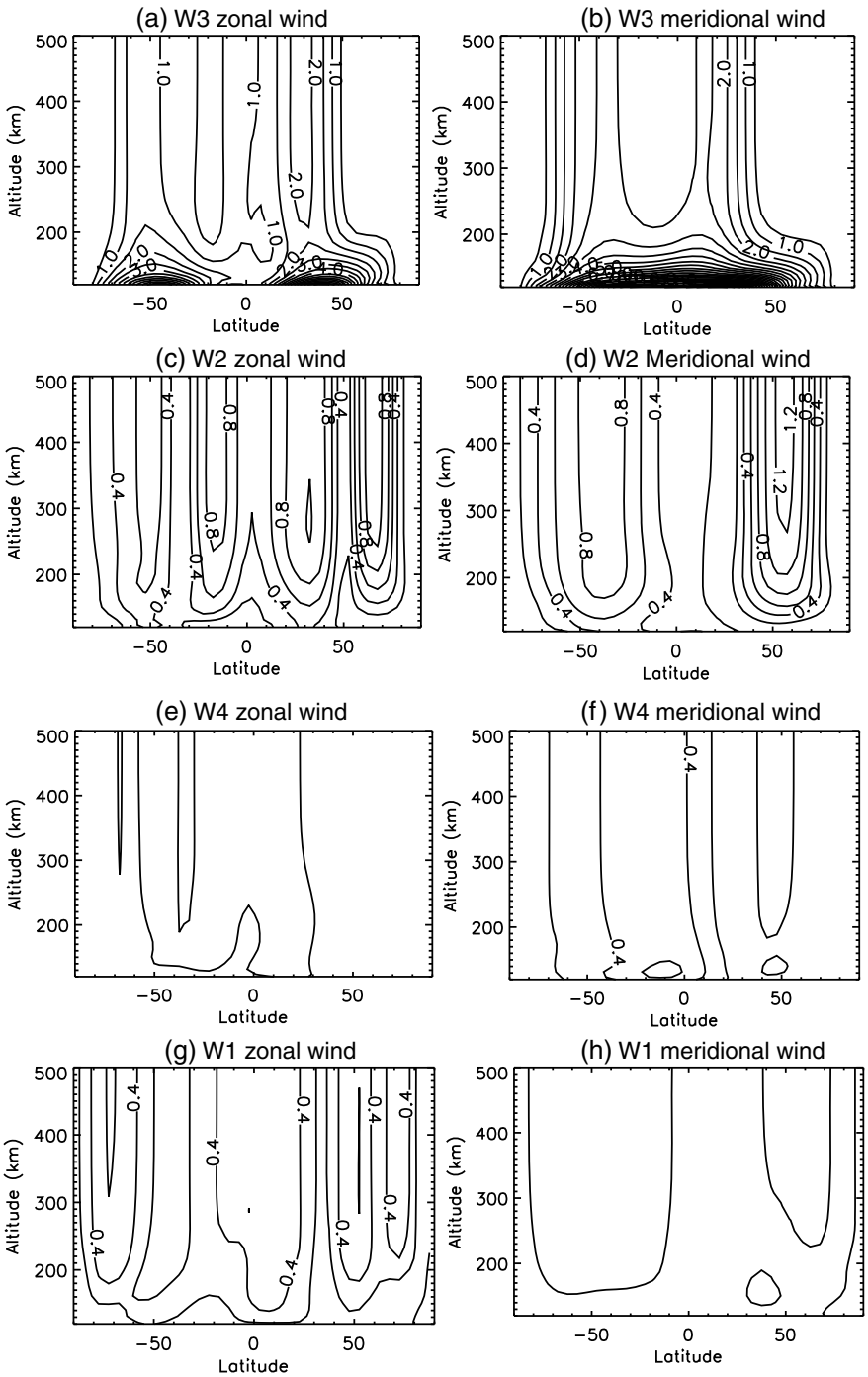

Figure 8. The amplitudes of the W3, W2, W4 and W1 QTDWs in thermospheric zonal and meridional wind at intervals of 0.5 m/s for W3 and 0.2 m/s for W2, W4, and W1, as a function of altitude and geographic latitude in the standard run using the IGRF magnetic field on model days 27–28.

QTDO of TEC all decrease dramatically once the magnetic field is set to be pure dipole and magnetic and geographic poles are aligned. It is noteworthy that both the W1 and S0 QTDOs of TEC are 0.02 TECU, respectively, in the aligned dipole field case (see Figures 6d and 6e). Although the geometry of the magnetic field can account for a large part of the zonal wavenumber broadening in the ionospheric plasma densities, other mechanisms of wavenumber broadening also need to be considered [*Forbes and Zhang*, 1997]. For example, new wavenumbers can also be generated through the QTDW modulations of the thermospheric $[O]/[N_2]$ ratio and meridional winds in the *F*-region [*England et al.*, 2010]. These potential factors will be addressed in future numerical work.

[20] As shown in Figure 7a, when the dynamo is completely turned off (or *E* is set to zero), there is still a nearly symmetric W3 QTDO in TEC (~0.02 TECU) near the EIA crests (dotted line). From Figure 7b, the W2 QTDO of TEC in the run without dynamo is ~0.02 TECU, which is smaller than that in the standard run case but greater

than that in the case with dynamo and an aligned magnetic dipole. This cannot be explained by the zonal wavenumber "interaction" of the dynamo effect. Other processes, such as QTDW induced variations in thermospheric [O]/[N_2] ratio and meridional winds at *F*-region altitudes [*England et al*., 2010], may have an effect (~20%) in the coupling between the MLT and the ionosphere in our numerical simulations. Their "interactions" with the background thermosphere structures [*Forbes and Zhang*, 1997] may account for the additional wavenumber broadening. Further numerical simulations are needed to fully resolve this issue.

[21] Furthermore, the QTDO in electric currents can exert an ion drag force on the neutral wind [*Richmond*, 1995]. Therefore, the wavenumber broadening effect in the ionosphere can be fed back to the neutral wind in the thermosphere. Figure 8 shows the W3, W2, W4, and W1 QTDWs of neutral zonal and meridional wind in the standard run. The W3 QTDW winds decrease with height and are <2 ms^{-1} above 200 km. The W2 QTDW wind components are of the order of 1 m s^{-1}, which are small considering the large background wind (tens of m/s) in the thermosphere [e.g., *Drob et al*., 2008] but comparable to the W3 components and are insignificant compared to the wavenumber broadening effect on the vertical drifts and plasma densities. The W4 QTDW in meridional wind is ~0.4 m s^{-1} in the thermosphere (Figure 8f) and the W1 QTDW zonal wind is ~0.4 m s^{-1} (Figure 8g). The occurrence of the QTDWs with other wave numbers (W2, W4, and W1) in the lower thermosphere in Figure 2 can be attributed to the QTDOs in ion drag exerted by the QTDOs in the plasma flow. For the aligned dipole case, the W2 component of the QTDW in the thermospheric zonal wind is 1 order of magnitude smaller (~0.08 m s^{-1}) than that in the standard run (not shown).

4. Discussions

[22] It appears that ionospheric QTDOs associated with the QTDWs at middle latitudes may be more susceptible to the zonal wavenumber broadening effect than are ionospheric oscillations associated with wave types that occur primarily at low latitudes [*Chang et al*., 2010]. There is a latitudinal effect in the zonal wavenumber broadening. For example, the ionospheric wavenumber broadening effect of the QTDW is more significant than that of the eastward wave number 1 ultra fast Kelvin (UFK) wave in the TIME-GCM. The E1 UFK wave is constrained to the tropics, and *Chang et al*. [2010] found negligible amplitudes for UFK ionospheric oscillations with wavenumbers such as E2 and S0. The dependence of the ionospheric wavenumber broadening on the latitude of the causative atmospheric wave can be attributed to the latitudinal variations of magnetic coordinates, magnetic field strength, and dip angle, as illustrated by Figures 3b, 5b, and 5d. In Figure 3b, the S1 feature peaks around 60°S and decreases toward the equator. In Figure 5b, the magnetic strength shows a strong S1 pattern around 50°S, and this pattern becomes much weaker near the equator. On the other hand, sin(I) has a peak of W1 at the equator and is about 30% of the peak value at southern mid latitudes. Thus, the net effect of the wavenumber "interaction" between the QTDW and the magnetic field has a latitudinal dependence and favors southern middle latitudes.

[23] In this paper, we take the QTDW as an example to illustrate how the geometry of the magnetic field is a potential factor to account for the additional zonal wavenumber components observed in the ionosphere. But this wavenumber broadening effect is not limited to the QTDW. Recently, *Fang et al*. [2012] suggested that their modeled longitudinal wave 1 feature (at a fixed local time) in the equatorial vertical E × B drift was created by the coupling between the migrating semidiurnal westward wavenumber 2 tide (SW2) and the geomagnetic field configuration. Apparently in their model, the S1 component of the geomagnetic field "interacts" with the SW2 tide to produce the wave 1 feature. Based on ion density measurements, *Kil et al*. [2012] showed persistent wavenumber 1, 2, 3, and 4 patterns in the ionosphere regardless of the geomagnetic activity condition and waves propagating from below. They also suggested that the creation of the wavenumber 1 and wavenumber 2 patterns in ionospheric plasma densities is associated with the geomagnetic field configuration.

[24] The actual magnetic field and the coupling between the neutral atmosphere and the ionosphere electrodynamics are far more complicated than just a wavenumber addition or subtraction between the QTDW and the configuration of the geomagnetic field. However, a wavenumber "interaction" analogous to that described by *Teitelbaum and Vial* [1991] can be viewed as a first-order approximation to this process. Depending on the latitudinal structure of the planetary waves and tides, this approximation is useful to explain the longitudinal variability of electric fields and plasma densities at periods of multiple days or at frequencies that are subharmonics of 1 day that is not seen in lower atmosphere planetary waves and tides, during geomagnetically quiet periods. We think that this is a plausible mechanism for the additional zonal wavenumbers observed in the ionosphere [*Apostolov et al*., 1995; *Forbes and Zhang*, 1997]. This also supports the suggestion of *Fang et al*. [2012] that the observed additional zonal wavenumbers in the ionosphere may not necessarily be generated by the commonly known tidal/planetary wave interactions.

[25] The wavenumber interaction between the QTDW and the magnetic field discussed in this paper should not be confused with the nonlinear interactions between the QTDW and tides. The interaction between the QTDW and tides often yields secondary waves that have frequencies and zonal wave numbers equal to the sum and difference of the primary waves, which is reproduced in the TIME-GCM runs [e.g., *Yue et al*., 2012a]. This is different from the QTDW with "new" zonal wavenumbers and the same period, which is the case for the interaction between the QTDW and the geomagnetic field. The exception is that the difference child wave produced by the interaction between the QTDW and the migrating diurnal tide can have a quasi 2 day period with zonal wavenumber E2 [*Palo et al*., 2007]. In all our TIME-GCM runs, the same migrating diurnal and semidiurnal tides from the GSWM are forced at the TIME-GCM lower boundary. We see very different responses for QTDOs of electric fields, vertical ion drifts, and TEC for zonal wavenumbers other than W3 in the standard run and the run with the aligned dipole. Thus, the enhanced QTDOs with W2, W4, and other zonal wavenumbers in the ionosphere in the standard run are not the results of the interaction between the QTDW and the migrating diurnal or semidiurnal tides.

[26] Recently, *Liu et al*. [2012] and *England et al*. [2012] provided substantial observational evidence that quasi 3 day wave signatures are present in the thermosphere/ionosphere system, producing variations with the same period in ionospheric parameters. This quasi 3 day wave and any other planetary waves are not included in our TIME-GCM runs, since they are not forced at the lower boundary or excited internally in the model. The addition of other planetary waves in the model along with the QTDW and the investigation of its impact in the ionosphere are beyond the scope of this paper and need further investigation.

5. Conclusion

[27] In this study, we study the zonal wavenumber broadening effect that is associated with the coupling between the QTDW in the MLT region and the ionosphere. We compare TIME-GCM results with the IGRF magnetic field with those from a model run in which the magnetic field is a pure dipole and the magnetic poles are aligned with the geographic poles. We demonstrate that the occurrence of additional zonal wave numbers of QTDOs in the ionospheric parameters, such as electric fields, vertical ion drifts, plasma densities, and TEC, is primarily caused by the configuration of the magnetic field. Earth's magnetic field (both its strength and dip angle) has zonal wavenumber 1 and higher-order structures in both geographic and magnetic coordinates. As a result, the neutral wind dynamo electric field and its associated vertical ion drift can be influenced by the wavenumber "interaction" between the W3 QTDW and the magnetic field (mainly S1). This also largely accounts for the additional wavenumbers seen in TEC or NmF2 observations. Using the QTDW as an example, the approximation proposed in this work of wavenumber summation and difference between the original wavenumber and stationary wavenumbers 1 and 2 in the magnetic field can also be applied to the interaction between any other planetary waves or tides and the ionosphere. The mechanism of wavenumber interaction is latitude dependent as a result of the configurations of magnetic coordinates, magnetic field strength, and dip angle in geographic coordinates. Thus, some planetary waves and tides may have a greater effect of wavenumber broadening than others depending on their latitudinal wind structure. The "new" wavenumber structures in the ionosphere can feed back onto the neutral wind in the thermosphere through ion drag, although this secondary effect is of minor importance for the QTDW because of its relatively small amplitude in the neutral thermospheric fields. All of the theories proposed in this work will be tested by comparing with observations in future work.

[28] **Acknowledgments.** The National Center for Atmospheric Research is supported by the National Science Foundation. We thank Astrid Maute for setting the aligned magnetic dipole field in the TIME-GCM and helpful discussions. We thank the anonymous reviewers of a previous draft of this paper for identifying points requiring clarification. This paper is also supported in part by NASA grants NNX10AQ59G, NNX08AQ91G, NNX09AJ83G, NNH08AH37I, and NNX09AN57G, NSF CEDAR grant ATM-0836386 and AGS-1138784, and the Center for Integrated Space Weather Modeling (CISM) which is funded by the STC Program of the National Science Foundation under agreement ATM-0120950. L. C. Chang was supported by grant NSC 101-2111-M-008-021-MY2 from the Taiwan National Science Council.

[29] Robert Lysak thanks the reviewers for their assistance in evaluating this paper.

References

Apostolov, E. M., D. Altadill, and L. F. Alberca (1995), Characteristics of quasi-2-day oscillations in the foF2 at northern middle latitude, *J. Geophys. Res.*, *100*, 12163–12171.

Chang, L. C., S. E. Palo, H.-L. Liu, T.-W. Fang, and C. S. Lin (2010), Response of the thermosphere and ionosphere to an ultra fast Kelvin wave, *J. Geophys. Res.*, *115*, A00G04, doi:10.1029/2010JA015453.

Chang, L. C., J.-Y. Liu, and S. E. Palo (2011a), Propagating planetary wave coupling in SABER MLT temperatures and GPS TEC during the 2005/2006 austral summer, *J. Geophys. Res.*, *116*, A10324, doi:10.1029/2011JA016687.

Chang, L. C., S. E. Palo, and H.-L. Liu (2011b), Short-term variability in the migrating diurnal tide caused by interactions with the quasi 2 day wave, *J. Geophys. Res.*, *116*, D12112, doi:10.1029/2010JD014996.

Chen, P.-R. (1992), Two-day oscillation of the equatorial ionization anomaly, *J. Geophys. Res.*, *97*, 6343–6357.

Drob, D. P., et al. (2008), An empirical model of the Earth's horizontal wind fields: HWM07, *J. Geophys. Res.*, *113*, A12304, doi:10.1029/2008JA013668.

England, S. L., S. Maus, T. J. Immel, and S. B. Mende (2006), Longitudinal variation of the E-region electric fields caused by atmospheric tides, *Geophys. Res. Lett.*, *33*, L21105, doi:10.1029/2006GL027465.

England, S. L., T. J. Immel, J. D. Huba, M. E. Hagan, A. Maute, and R. DeMajistre (2010), Modeling of multiple effects of atmospheric tides on the ionosphere: An examination of possible coupling mechanisms responsible for the longitudinal structure of the equatorial ionosphere, *J. Geophys. Res.*, *115*, A05308, doi:10.1029/2009JA014894.

England, S. L., G. Liu, Q. Zhou, T. J. Immel, K. K. Kumar, and G. Ramkumar (2012), On the signature of the quasi-3-day wave in the thermosphere during the January 2010 URSI World Day Campaign, *J. Geophys. Res.*, *117*, A06304, doi:10.1029/2012JA017558.

Fang, T.-W., T. Fuller-Rowell, R. Akmaev, F. Wu, H. Wang, and D. Anderson (2012), Longitudinal variation of ionospheric vertical drifts during the 2009 sudden stratospheric warming, *J. Geophys. Res.*, *117*, A03324, doi:10.1029/2011JA017348.

Forbes, J. M., and X. Zhang (1997), Quasi-2-day oscillation of the ionosphere: A statistical study, *J. Atmos. Terr. Phys.*, *59*(9), 1025–1034.

Gledhill, J. A. (1976), Aeronomic effects of the South Atlantic Anomaly, *Rev. Geophys.*, *14*(2), 173–187, doi:10.1029/RG014i002p00173.

Gurubaran, S., T. K. Ramkumar, S. Sridharan, and R. Rajaran (2001), Signatures of quasi-2-day planetary waves in the equatorial electrojet: Results from simultaneous observations of mesospheric winds and geomagnetic field variations at low latitudes, *J. Atmos. Sol. Terr. Phys.*, *63*, 813–821.

Hagan, M. E., M. D. Burrage, J. M. Forbes, J. Hackney, W. J. Randel, and X. Zhang (1999), GSWM-98: Results for migrating solar tides, *J. Geophys. Res.*, *104*, 6813–6828.

Hagan, M. E., A. Maute, R. G. Roble, A. D. Richmond, T. J. Immel, and S. L. England (2007), Connections between deep tropical clouds and the Earth's ionosphere, *Geophys. Res. Lett.*, *34*, L20109, doi:10.1029/2007GL030142.

Heelis, R. A. (2004), Electrodynamics in the low and middle latitude ionosphere: a tutorial, *J. Atmos. Sol. Terr. Phys.*, *66*, 825–838.

International Association of Geomagnetism and Aeronomy, Working Group V-MOD, Participating members, C. C. Finlay et al. (2010), International Geomagnetic Reference Field: The eleventh generation, *Geophys. J. Int.*, *183*(3), 1216–1230, doi:10.1111/j.1365-246X.2010.04804.x.

Immel, T. J., E. Sagawa, S. L. England, S. B. Henderson, M. E. Hagan, S. B. Mende, H. U. Frey, C. M. Swenson, and L. J. Paxton (2006), Control of equatorial ionospheric morphology by atmospheric tides, *Geophys. Res. Lett.*, *33*, L15108, doi:10.1029/2006GL026161.

Ito, R., S. Kato, and T. Tsuda (1986), Consideration of an ionospheric wind dynamo driven by a planetary wave with a two-day period, *J. Atmos. Terr. Phys.*, *48*, 1–13.

Kil, H., W. K. Lee, Y.-S. Kwak, S.-J. Oh, L. J. Paxton, and Y. Zhang (2012), Persistent longitudinal features in the low-latitude ionosphere, *J. Geophys. Res.*, *117*, A06315, doi:10.1029/2012JA017570.

Lastovicka, J. (2006), Forcing the ionosphere by waves from below, *J. Atmos. Sol. Terr. Phys.*, *68*, 479–497.

Limpasuvan, V., D. L. Wu, M. J. Schwartz, J. W. Waters, Q. Wu, and T. L. Killeen (2005), The two-day wave in EOS MLS temperature and wind measurements during 2004–2005 winter, *Geophys. Res. Lett.*, *32*, L17809, doi:10.1029/2005GL023396.

Liu, G., S. L. England, T. J. Immel, K. K. Kumar, G. Ramkumar, and L. P. Goncharenko (2012), Signatures of the 3-day wave in the low-latitude and midlatitude ionosphere during the January 2010 URSI World Day campaign, *J. Geophys. Res.*, *117*, A06305, doi:10.1029/2012JA017588.

Liu, H.-L., E. R. Talaat, R. G. Roble, R. S. Lieberman, D. M. Riggin, and J. H. Yee (2004), The 6.5-day wave and its seasonal variability in the middle and upper atmosphere, *J. Geophys. Res.*, *109*, D21112, doi:10.1029/2004JD004795.

Liu, H.-L., W. Wang, A. D. Richmond, and R. G. Roble (2010), Ionospheric variability due to planetary waves and tides for solar minimum conditions, *J. Geophys. Res.*, *115*, A00G01, doi:10.1029/2009JA015188.

Palo, S. E., R. G. Roble, and M. E. Hagan (1998), Time-GCM results for the quasi two-day wave, *Geophys. Res. Lett.*, *25*, 3783–3786.

Palo, S. E., J. M. Forbes, X. Zhang, J. M. Russell III, and M. G. Mlynczak (2007), An eastward propagating two-day wave: Evidence for nonlinear planetary wave and tidal coupling in the mesosphere and lower thermosphere, *Geophys. Res. Lett.*, *34*, L07807, doi:10.1029/2006GL027728.

Pancheva, D., L. F. Alberca, and B. A. de la Morena (1994), Simultaneous observation of the quasi-two-day variations in the lower and upper ionosphere over Europe, *J. Atmos. Terr. Phys.*, *56*, 43–50.

Pancheva, D.V., et al. (2006), Two-day wave coupling of the low-latitude atmosphere–ionosphere system, *J. Geophys. Res.*, *111*, A07313, doi:10.1029/2005JA011562.

Richmond, A. D., E. C. Ridley, and R. G. Roble (1992), A thermosphere/ionosphere general circulation model with coupled electrodynamics, *Geophys. Res. Lett.*, *19*, 601–604.

Richmond, A. D. (1995), The ionospheric wind dynamo: Effects of its coupling with different atmospheric regions, *Geophys. Monogr.*, *87*.

Roble, R. G., E. C. Ridley, A. D. Richmond, and R. E. Dickinson (1988), A coupled thermosphere/ionosphere general circulation model, *Geophys. Res. Lett.*, *15*, 1325–1328.

Roble, R. G., and E. C. Ridley (1994), A thermosphere-ionosphere-mesosphere-electrodynamics general circulation model (TIME-GCM): Equinox solar cycle minimum simulations (30–500 km), *Geophys. Res. Lett.*, *21*, 417–420.

Salby, M. L. (1981), The 2-day wave in the middle atmosphere: Observations and theory, *J. Geophys. Res.*, *86*(C10), 9654–9660.

Takahashi, H., L. M. Lima, C. M. Wrasse, M. A. Abdu, I. S. Batista, D. Gobbi, R. A. Buriti, and P. P. Batista (2005), Evidence on 2–4 day oscillations of the equatorial ionosphere h′F and mesospheric airglow emissions, *Geophys. Res. Lett.*, *32*, L12102, doi:10.1029/2004GL022318.

Teitelbaum, H., and F. Vial (1991), On tidal variability induced by nonlinear interaction with planetary waves, *J. Geophys. Res.*, *96*, 14169–14178.

Tunbridge, V. M., D. J. Sandford, and N. J. Mitchell (2011), Zonal wave numbers of the summertime 2 day planetary wave observed in the mesosphere by EOS Aura Microwave Limb Sounder, *J. Geophys. Res.*, *116*, D11103, doi:10.1029/2010JD014567.

Wu, D. L., P. B. Hays, W. R. Skinner, A. R. Marshall, M. D. Burrage, R. S. Lieberman, and D. A. Ortland (1993), Observations of the quasi 2-day wave from the high resolution Doppler imager on UARS, *Geophys. Res. Lett.*, *20*(24), 2853–2856.

Yue, J., H.-L. Liu, and L. Chang (2012a), Numerical investigation of the quasi-two-day wave in the mesosphere and lower thermosphere, *J. Geophys. Res.*, *117*, D05111, doi:10.1029/2011JD016574.

Yue, J., W. Wang, H.-L. Liu, and A. Richmond (2012b), Quasi-two-day wave coupling of the mesosphere and lower thermosphere-ionosphere in the TIME-GCM: Two-day oscillations in the ionosphere, *J. Geophys. Res.*, *117*, A07305, doi:10.1029/2012JA017815.